Applied Thermal Engineering 305 (2026) 132845

Contents lists available at ScienceDirect

Applied Thermal Engineering

journal homepage: www.elsevier.com/locate/apthermeng

Research Paper

New method for fast heat transfer analysis of PCM cross sections with integrated finned tubes☆

Matias Pezo *, Wolf-Dieter Steinmann, Andrea Gutierrez

Institute of Engineering Thermodynamics, German Aerospace Center (DLR), Pfaffenwaldring 38-40, 70569 Stuttgart, Germany

ARTICLE INFO

Keywords:
Phase change material
COMSOL
Longitudinal finned tube heat exchanger
Simplified model

ABSTRACT

State-of-the-art Latent Heat Thermal Energy Storage (LHTES) units use extended heat transfer surfaces to compensate for the typically low thermal conductivity of cost-effective phase change materials (PCMs). The analysis of such surfaces currently depends heavily on numerical simulations. However, due to high computational costs, this approach cannot be practically scaled to analyze complete LHTES storage units. To overcome this limitation, this study proposes a computationally efficient alternative for the analysis of PCM storage systems. In this new methodology, finned geometries are characterized using a novel, purely geometric distance-based framework. This approach serves as the foundation for a simplified model that entirely eliminates the need for additional numerical calibration.

To achieve this, four distinct longitudinally extruded fin profiles (24-Branch-Star, Organic, Snowflake, and 6-Branch-Star) with identical fin fractions were evaluated. The methodology translates complex 2D fin cross-sections into 1D Cumulative Distribution Functions (CDFs) based on shortest-path heat transfer distances. A simplified transient model for quasi-isothermal fins was subsequently developed and validated against reference 2D numerical simulations.

Results demonstrate that the contact perimeter between PCM and fin P_{fin} is inversely proportional to the melting time, whereas the novel average distance between the PCM and the fin $\overline{D}_{PCM-fin}$ exhibits a direct linear correlation with the phase change time. Both parameters are therefore proven to be reliable predictors for the design of finned profiles. Furthermore, the simplified model for quasi-isothermal fins accurately predicted the transient liquid fraction with a mean absolute error $\overline{\Delta f_l}$ of less than 0.026, while delivering speedup ratios R_{speed} between 77 and 183 times compared to the reference 2D numerical simulations. The proposed time-ratio efficiency metric revealed that while highly branched profiles yield faster melting times, their necessary branch slenderness imposes significant internal conduction resistance. Finally, this novel distance framework provides a highly reliable, numerically-independent tool, eliminating computational bottlenecks and enabling the rapid algorithmic optimization of LHTES fin geometries.

1. Introduction

The increasing share of fluctuating renewable energy sources, coupled with increasing global energy demand, has focused engineering interest on new forms of energy storage [1]. Among the various power-to-power technologies, Carnot Batteries are thermo-mechanical storage systems combining thermal energy storage with thermal power cycles [2,3]. Surplus electric energy from the grid can be stored as thermal energy and used at a more convenient time to operate the power cycle. The most efficient Carnot Battery configurations utilize a heat pump to charge the thermal storage system. To achieve high round-trip efficiencies, it is crucial to minimize entropy generation during these charging and discharging heat transfer processes. This makes Latent Heat Thermal Energy Storage (LHTES) particularly advantageous for Rankine cycles, where the majority of energy transfer occurs isothermally during condensation and evaporation. By utilizing a phase change material with a melting point close to the saturation temperature of the steam, LHTES enables heat transfer across exceptionally small temperature differences [4].

A critical challenge in implementing LHTES systems is designing an effective heat transfer mechanism between the phase change material

☆ This article is part of a Special issue entitled: 'ECOS2025' published in Applied Thermal Engineering.

* Corresponding author.
E-mail address: matias.pezoperez@dlr.de (M. Pezo).

https://doi.org/10.1016/j.applthermaleng.2026.132845
Received 10 March 2026; Received in revised form 29 July 2026; Accepted 13 August 2026

Nomenclature

Symbols & Abbreviations

A	Area, [m^2]
c_p	Heat capacity at constant pressure, [J kg^{-1} K^{-1}]
CDF	Cumulative Distribution Function
d	Diameter, generalized distance, [mm]
D	Distance, [mm]
$\overline{D}$	Average Distance, [mm]
f	Fraction, [−]
H	Height, [mm]
HTF	Heat Transfer Fluid
k	Thermal conductivity, [W m^{-1} K^{-1}]
L	Latent heat of fusion, [kJ kg^{-1}]
LHTES	Latent Heat Thermal Energy Storage
PC	Phase Change
PCM	Phase Change Material
$\dot{Q}$	Heat transfer rate, [W]
$\dot{q}$	Heat flux, [kW m^{-2}]
s	Position of the phase change front, [mm]
Ste	Stefan number, [−]
T	Temperature, [°C]
t	Time, [s]

Subscripts

eff	Effective, apparent
fin	Fin
hex	Hexagon
l	Liquid
m	Melting
max	Maximum
min	Minimum
PCM	PCM
s	Solid
time	Time
tube	Tube

Greek symbols

η	Efficiency, [−]
λ	Positive root of the transcendental eq., [−]
ρ	Density, [kg m^{-3}]
ε	Convective enhancement factor, [−]

(PCM) and the heat transfer fluid (HTF) to overcome the inherently low thermal conductivity of cost-effective PCMs. Among available configurations, the shell-and-tube heat exchanger has achieved the highest technological maturity. In this design, the PCM mass is contained by the shell, and tubes are used to charge and discharge thermal energy using the HTF. This study will use the vertical staggered tube layout since it prevents isolated liquid volumes by ensuring that the melting progresses from the top to the bottom during charging, and solidification occurs from the bottom up during discharging [5].

PCMs can be classified based on their chemical composition, melting temperature and energy storage capabilities. Inorganic salts have relatively high energy densities and melting temperatures compatible with Rankine cycles. Nevertheless, cost-effective PCMs have low thermal conductivities, limiting the energy input and output of the storage. To overcome this challenge, the contact area of the tubes is extended using aluminum fins [6]. Fins can be classified depending on their design as annular/parallel or longitudinal/axial fins. Fig. 1 shows two categories of the most commonly used fin designs in the literature, which have been thoroughly reviewed by previous studies [7–9]. Former studies have shown that independent of the geometry, fins represent between 30 and 40% of the capital costs of the LHTES module, making them a crucial optimization aspect [10].

The moving-boundary problems, also called Stefan-problems, were first formalized by Josef Stefan in the late 19th century. The similarity analytical solution described by Neumann a few decades before can be found in the books by Alexiades and Solomon [11], and Mehling and Cabeza [6]. The classical similarity solution to this formulation, restricted to semi-infinite domains with constant thermophysical properties, underlies the catalogue of exact solutions compiled for simple one-dimensional geometries, planar, cylindrical, and spherical, by Carslaw and Jaeger [12]. Beyne extended this Neumann-type approach to several derived geometries relevant to LHTES design, including planar and tube-in-tube (shell-and-tube without fins) enclosures, pipe-in-pipe configurations, cylindrical PCM modules immersed in an HTF shell, and spherically encapsulated PCM immersed in an HTF packed bed [13]. For finned structures, however, no geometry-independent Neumann-type formulation has been proposed to date. The closest attempt was Bauer, who developed an analytical model for the solidification of

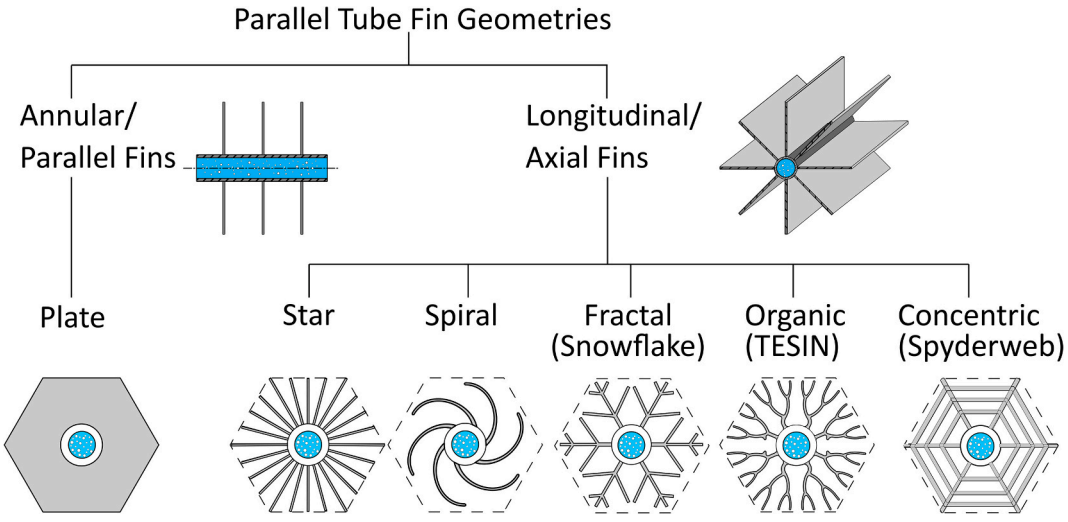

Fig. 1. Classification of different fin geometries for parallel tube heat exchangers. (Adapted from [5]).

LHTES systems using two specific parallel-fin cross-sections (rectangular and circular); the model assumed conduction-dominated heat transfer and effective thermophysical properties for the fin-PCM mixture, and was calibrated by fitting the resulting weighted analytical solution against CFD simulations of each geometry [14]. Consequently, extending this approach to a new fin cross-section requires a new set of reference simulations for recalibration.

Fixed-grid methods remain the most common alternative for incorporating arbitrary finned profiles into simulation, using either the effective/apparent heat capacity method, the enthalpy method (developed by Voller [15]), or the heat source term method. In contrast to quasi-analytical formulations, fixed-grid methods require solving the energy equation, and where natural convection is considered, the momentum equation, at every element of the discretized domain, substantially increasing the computational cost compared to the geometric approach proposed in this paper. Consequently, most studies addressing realistic finned tube geometries have instead relied on such numerical simulations, resolving the coupled thermal and, where relevant, fluid-dynamic behavior of the storage unit in detail.

The effects of natural convection are often neglected although their importance depends strongly on the used layout and fin design. Vogel and Johnson [16] used numerical simulations to evaluate the effect of fin design and tube length on four different fin profiles using $NaNO_3$ as PCM. One of them (axial 230) was evaluated for three different fin heights to measure the effects of this parameter on natural convection. Their results showed non-neglectable effects for geometries with large tube spacing and low fin fraction, whereas for configurations with small tube spacing, high fin fraction and short tube lengths, natural convection was found negligible. Vogel, Keller [17] developed a computationally less expensive LHTES-calculation tool calibrated with an ANSYS Fluent model. The tool used an effective material of PCM and fins to reduce the number of elements where the differential equations had to be solved. The properties, such as the thermal conductivity, density, and heat capacity, of the effective material were calculated following the factor of parallelism proposed by Tay, Belusko [18], to describe how parallel or in series the heat was transferred within the PCM-fin mixture. The calculation of this factor requires previous CFD or experimental calibration, which is very time-consuming when a wide variety of fin designs are evaluated. Furthermore, even though the results delivered by the tool were accurate, the model could be simplified for faster calculations considering a quasi-stationary state, and therefore, not having to solve the differential equations describing the PCM volume. Sciacovelli, Gagliardi [19] studied two types of fractal (Y-fin) designs with single and double bifurcations on a vertical layout. The geometry was parametrically optimized using the length and bifurcation angles, maintaining the cross-sectional area of the fin to maximize the heat flux given an operating time constraint.

Pizzolato, Sharma [20] introduced a methodology to obtain 2D topologically optimized fins on a horizontal layout assessing both, melting and solidification processes, and comparing the results considering non-neglectable and neglectable natural convection. Because of the chosen layout, the resulting fins do not have an even distribution of the fin material, they instead follow non-trivial paths to reduce the solidification time. The study of topologic finned structures continued assessing the 3D branch distribution of the topologically optimized fins by Pizzolato, Sharma [21]. Two minimization approaches were proposed, first the residual energy of the storage after a given time, and second the solidification time. Although the 3D results outperformed those of the 2D approach, the high complexity of the obtained structures makes it difficult to manufacture them without additive manufacturing techniques, which currently are too costly for applications at industrial scale. Ge, Humbert [22] studied arrays of four finned tubes, comparing topologically optimized fins to star fins using CFD simulations, and experimentally using 3D printed fins and an acrylic shell. Three different paraffins with melting temperatures below 30 °C were used as PCMs. The topological fin had shorter solidification times but the star profile used as a benchmark was not optimized. Wang, Zadeh [23] compared a variety of star and topologically optimized fin profiles for the melting of a paraffin-based PCM. For the optimization, the heat transfer during phase change was maximized. While maintaining the same fin material for all profiles, the topological approach presented slightly shorter melting times than the best-performing star profile. When the fin fraction was increased, the melting time decreased but so did the storage capacity because of the lower PCM mass ratio.

A fundamental limitation of these existing reduced-order and analytical models stems from the current choice of geometric descriptors. Traditional heat exchanger metrics, such as fin thickness, height, number of branches, or bifurcation angles, are intrinsically tied to specific fin topologies (e.g., star, spiral, fractal, organic, or concentric configurations). A critical research gap persists: a unified geometric descriptor that can be universally applied across entirely distinct topological families remains missing from the literature. Regardless of the chosen cross-sectional complexity, all profiles share a single, fundamental physical constraint: thermal energy must flow from the tube wall, conduct through the fin, and diffuse into the surrounding PCM mass. Existing characterization frameworks fail to capture this universal spatial transport path natively, forcing reduced-order models to rely on tedious, case-by-case numerical recalibrations. A generalized method capable of extracting a common geometric descriptor from arbitrary 2D cross-sections is therefore essential to bridge this gap and unlock rapid, automated LHTES design optimization. Table 1 summarizes the characteristics of the above-mentioned investigations.

This paper introduces a new methodology to characterize complex fin geometries by alternative parameters which do not require a CFD analysis for calibration thus reducing the computational cost significantly and providing the basis for an automated optimization of fin LHTES geometries. To achieve this, the specific objectives are outlined as follows:

- To introduce a geometric spatial translation method that maps complex 2D fin geometries into 1D Cumulative Distribution Functions (CDFs).
- To evaluate the predictive reliability of these geometric parameters against reference 2D numerical simulations.
- To develop and validate a simplified transient model based on the CDF framework that accurately predicts the temporal evolution of the liquid fraction and boundary heat flux for quasi-isothermal fins.
- To propose metrics capable of extending the quasi-isothermal simplified model approach to real fins.

In this paper, four distinct finned tube cross-sections are modeled, each maintaining an identical fin fraction, to evaluate how the spatial distribution of the fin material governs the phase change dynamics. The

Table 1
Summary of investigations cited in the introduction.

Study	PCM (T_m [°C])	PC*	Type of fin	Layout
[16]	$NaNO_3$ (306)	S&M	A (Organic, Snowflake, Star) & P (Plates)	V-ST
[17]	$NaNO_3$ (306) KNO3- $NaNO_3$ (222)	S&M	A (Organic) & P (Plates)	V-ST
[19]	Paraffin wax (57)	S	A (Fractal)	V-ST
[20]	Dimensionless PCM (−)	S	A (2D Top. opt.)	H-ST
[21]	Dimensionless PCM (−)	S	A (2D Top. opt.) & O (3D Top. opt.)	V-ST
[22]	3 paraffins: RT18HC (18), RT22HC (22), RT25HC (24)	S	A (2D Top. opt. & 10-Branch-Star)	V-TA
[23]	RT50 Paraffin (51)	M	A (Star & 2D Top. opt.)	H-ST

* *Studied Phase Change (PC) can either be Solidification (S), Melting (M), or both (S&M). The type of fin can either be Axial (A), Parallel (P) or Other (O). The layout can be Vertical (V), Horizontal (H) combined with the assessment of a Single Tube (ST) or Tube Arrays (TA).*

comparison of these fin profiles is motivated by the use of simplified PCM–fin ratio models discussed in the introduction. The ultimate objective is to develop a geometry-based calibration capable of predicting the thermal performance of a given fin design. Such an approach would eliminate the need for a reference numerical simulation (e.g., ANSYS or COMSOL) for each new geometry, thereby enabling the rapid evaluation of a wide range of fin designs tailored to specific thermal demands.

The eutectic mixture of KNO_3 -$NaNO_3$ with a melting temperature of 222 °C will be used as PCM. The characterization results will be used as a first step for the development of a multi-scale simulation tool shown in Fig. 2, which describes three different levels that compose the LHTES module: (i) a thin transverse slice representing the cross section, (ii) a single finned tube surrounded by PCM, and (iii) the complete storage unit. The present work focuses on the first level, investigating the influence of fin material distribution on the phase change rate under a fixed temperature boundary condition at the tube wall, with the PCM initially in a single phase and subsequently undergoing melting.

2. Methodology

2.1. Problem statement

In the context of LHTES for Carnot battery applications, maintaining a narrow temperature difference between the heat transfer fluid and the storage unit temperature is crucial to increase the overall power-to-power efficiency, as the exergy destruction during charging and discharging cycles is reduced. Thermodynamically, this narrow operational temperature window implies that the sensible heat stored or released by the system is small compared to the latent heat of fusion. This relationship is characterized by the Stefan number *Ste*, defined as the ratio of sensible heat to latent heat [11]:

$$Ste = \frac{c_p \Delta T}{L_m} \tag{1}$$

where c_p is the specific heat capacity of the PCM, ΔT is the temperature difference and L_m is the latent heat of fusion.

In previous approaches [17,18,24], one of the decisive parameters when describing the finned tube heat exchangers is the relative fin fraction. This relation indicates the ratio of fin material with respect to the PCM and the tube. Eq. (2) shows the definition for a two-dimensional case, which can be calculated as the ratio between the fin and the total hexagonal area:

$$f_{fin} = \frac{A_{fin}}{A_{hex}} = \frac{A_{fin}}{A_{fin} + A_{PCM} + A_{tube}} \tag{2}$$

In this context, Fig. 3 presents the four fin designs considered in this study. All configurations share the same fin fraction, fin diameter, and tube diameter, and differ only in the spatial distribution of the fin material. The selected fin fraction is based on the "Organic" design proposed within the TESIN project, which had a discharge time of 15 min [25]. In particular, the designs proposed in this paper have a slightly enlarged diameter than the one used on the TESIN project.

The storage unit consists of a vertical bundle of parallel tubes utilizing longitudinally extruded fins. As previously described in the fin classification (Fig. 1), annular-parallel configurations utilize plates and therefore possess a fin spacing. In contrast, the extruded fins evaluated here are continuous along the axial length. Consequently, axial fin spacing is not applicable; the only relevant spacing is the tube spacing, which is determined entirely by the hexagonal boundary of the fins. The present methodology is strictly bounded to a 2D cross-section; macro-scale shell dimensions are therefore outside the scope of this geometric framework.

Fig. 4 shows the geometric parameters used to define this 2D domain. As observed in the top view of the DLR-TESIN demonstrator (Fig. 4, left), the densely packed vertical tubes form a honeycomb arrangement. Consequently, a single finned tube can be isolated and modeled within a hexagonal symmetry boundary. For the purposes of this study, the "fin diameter" is defined as equal to the hexagon internal diameter. This is because the physical gaps between the fin tops of adjacent tubes in the real-world array are limited strictly to the tolerances necessary for mechanical assembly. The fundamental dimensions for the tube and fin structures evaluated in this study are detailed in Table 4.

Table 2 summarizes the thermophysical properties of the materials considered in this study. The eutectic mixture of KNO_3-$NaNO_3$ was selected as the phase change material (PCM) due to its proven potential for industrial thermal energy storage applications, as demonstrated in previous prototype systems such as flat-plate heat exchangers [26], the *PCM-Flux Concept* [27], and the *Rotating Drum Concept* [28]. This PCM is particularly suitable because of its relatively high and sharp melting temperature of 222 °C, its good thermal stability, and its cost-effective availability.

In addition to the PCM properties in both solid and liquid phases, the thermophysical properties of stainless steel and aluminum are included, as these materials are commonly used in heat exchanger tubes and fins. A quasi-isothermal material is also introduced to represent an idealized fin with extremely high thermal conductivity. This fictitious material is used as a benchmark to assess the upper performance limit of the finned heat exchanger configuration.

To establish a consistent physical framework for both the reference numerical simulations and the simplified geometric model, the following general assumptions are applied to the heat exchanger control volume:

- Two-dimensional heat transfer: The system is modeled as a 2D cross-section. Axial temperature gradients and end-effects along the vertical length of the tubes are not taken into consideration.

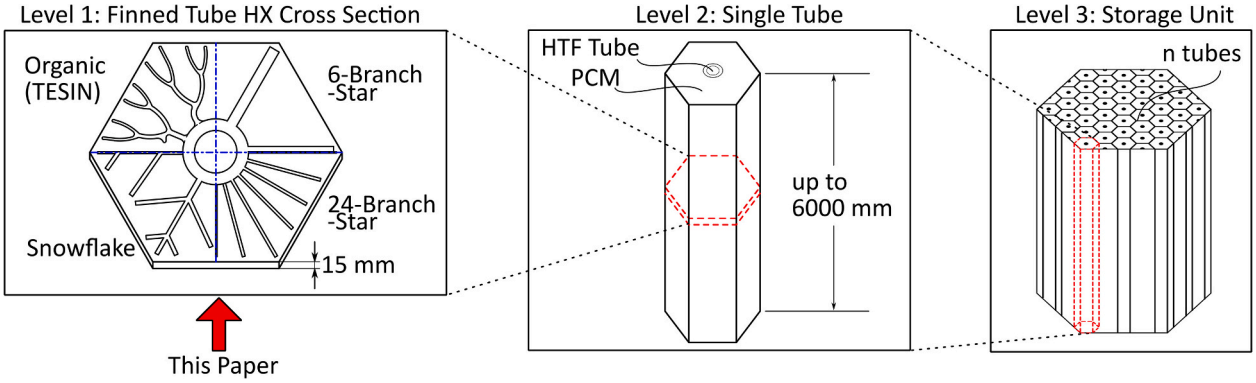

Fig. 2. Hierarchical Multi-Scale Modeling Approach.

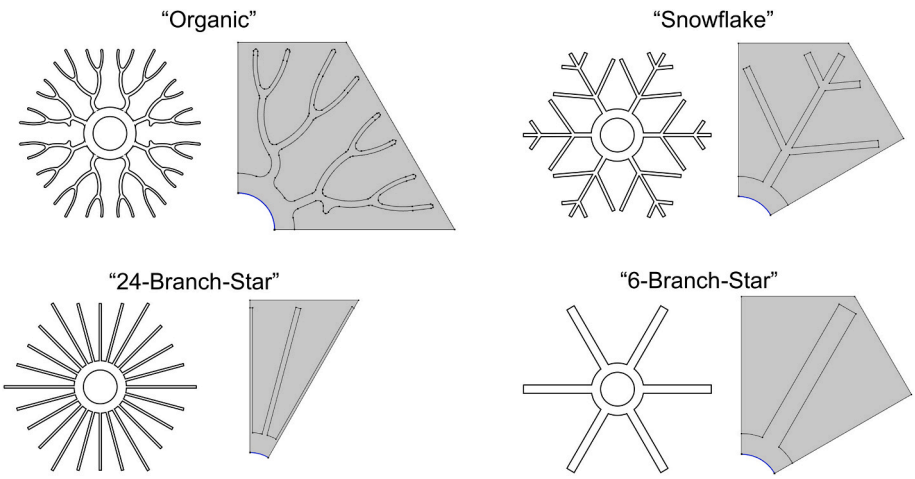

Fig. 3. Cross-section of the studied finned-tube heat exchangers and simplified geometry used in COMSOL.

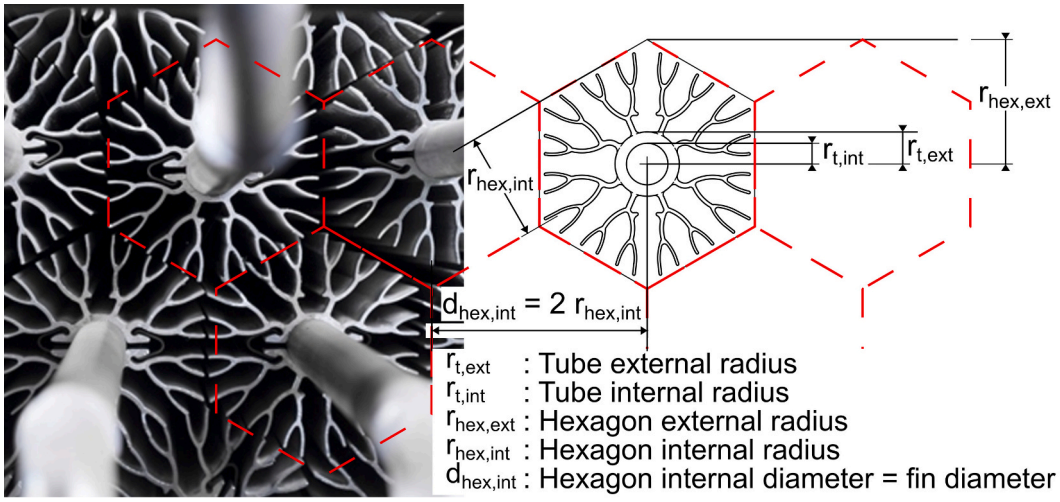

Fig. 4. Schematic illustrating the geometric parameters that define the 2D computational domain. Left: Top view of the vertical DLR-TESIN storage unit demonstrator, showing the array of finned tubes. Source: ©Knauf Interfer. Right: Definition of the hexagonal boundary, and the fin and tube radii.

Table 2
Thermophysical properties of the materials used in this study. The quasi-isothermal material represents an idealized fin with extremely high thermal conductivity.

Material	Solid PCM	Liquid PCM	Stainless Steel	Aluminum	Quasi-isothermal material
Th. Conduct., k [W m^{-1} K^{-1}]	0.435	0.457	15	210	20,000
Heat Capacity, c_p [J kg^{-1} K^{-1}]	1350	1492	500	1020	1020
Density, ρ [kg m^{-3}]	2017.5		7900	2700	2700
Melting Temperature, T_m [°C] ([K])	222 (495.15)		–	–	–
Latent Heat, L_m [kJ kg^{-1}]	108		–	–	–
Dynamic Viscosity, μ [Pa s]	–	$5.8 \cdot 10^{-3}$	–	–	–
Thermal Expansion Coef., β [K^{-1}]	–	$3.5 \cdot 10^{-4}$	–	–	–
Source	[27,29–31]		[32]	[27]	–

- Thermophysical properties: The latent heat of fusion, melting temperature, and density are considered constant. Thermal conductivity and heat capacity are considered constant within each phase. Density is strictly held constant to prevent artificial variations in the mass of the PCM control volume during phase change.
- Conduction-dominated heat transfer: Radiation and natural convection within the liquid PCM are neglected. Since the orientation of the tubes is vertical, two components are expected to be relevant for natural convection; first, the relative position across the tube length, and second, the interaction with neighboring finned tubes affected by external boundary conditions (edges of the storage unit). The analysis of natural convection would require the calculation of at least one pipe over the entire length, which would lead to considerable computational efforts if a typical length of 6 m is calculated. For these reasons and because of the constant density consideration, natural convection will be neglected, hence the continuity and momentum equations will not be considered. This is expected to have a low impact on the quality of the results, since the diameter, length of the tube and fin fraction follow the trend suggested by Vogel and Johnson [16] to have a diffusion-dominated heat transfer. For the same reasons, buoyancy effects are also neglected as previously proposed by Sciacovelli, Gagliardi [19]

- Perfect thermal contact: Thermal contact resistance at the interfaces between the heat transfer fluid and the tube, the tube and the fin, and the fin and the PCM is assumed to be zero.
- Initial condition: At time $t = 0$, the entire domain is assumed to be at a uniform temperature 10 K below the melting temperature (212 °C). Based on the PCM properties shown on Table 2, this yields a Stefan number of approximately 0.13.
- Inner tube boundary condition: A constant temperature boundary condition of 232 °C is applied at the inner tube wall, representing phase change of the heat transfer fluid. This boundary condition is represented by the blue line in Fig. 3.
- Adiabatic outer boundaries: The external hexagonal boundaries of the computational domain are defined as adiabatic symmetry planes, representing a periodic array of identical finned tubes within the LHTES unit.

Based on the mentioned assumptions, the range of applicability of the proposed geometric model is strictly bounded to the 2D cross-sectional domain, corresponding to the Level 1 abstraction illustrated in Fig. 2. Mathematically, this formulation evaluates a computationally thin slice of the extruded fin with a virtually negligible height (15 mm). This discrete height dimension is retained strictly to facilitate the calculation of the fin perimeter based on the PCM-fin contact area. While real full-scale vertical LHTES units will inevitably develop axial temperature gradients, these effects are actively suppressed in the present methodology by the assumption of a phase-changing heat transfer fluid, which maintains a constant temperature boundary condition along the entire inner tube wall. By restricting the physical model to a conduction-dominated slice with negligible height, the results presented herein represent a conservative baseline; in a macroscopic physical system, the onset of buoyancy-driven natural convection along the vertical axis would only serve to accelerate heat transfer and reduce the overall melting time. Consequently, this conduction-driven approach provides a reliable framework for LHTES system design, ensuring that any resulting geometric configurations inherently include a conservative safety margin for overall heat transfer performance.

2.2. Reference numerical model (COMSOL)

The commercial simulation tool COMSOL-Multiphysics® [33] was used for the reference simulations. The Heat Transfer and CAD-Import modules were used to carry out a time-dependent study of the melting process. To reduce the computational cost, symmetry was used to solve only the simplified structure shown on the right of each fin profile in Fig. 3. The phase change is modeled using the apparent heat capacity method with a finite temperature glide.

The mathematical formulation implemented in COMSOL follows the description provided in the Heat Transfer Module documentation [33]. The transient energy equation is solved using PCM properties computed via the apparent heat capacity formulation:

$$\rho c_{p,eff}\frac{\partial T}{\partial t} = \vec{\nabla}\cdot(k\vec{\nabla}T) \tag{3}$$

where ρ, $c_{p,eff}$, T, and t represent density, effective (or apparent) heat capacity, temperature, and time respectively. A temperature glide ΔT of 2 K is prescribed around the melting temperature T_m, avoiding the explicit inclusion of the latent heat term in the energy equation. Within this interval, the liquid fraction is defined as:

$$f_l(T) = \begin{cases} 0, & T < T_m - \dfrac{\Delta T}{2} \\ 0^+ \ldots 1^-, & T_m - \dfrac{\Delta T}{2} \le T < T_m + \dfrac{\Delta T}{2} \\ 1, & T \ge T_m + \dfrac{\Delta T}{2} \end{cases} \tag{4}$$

where the superscripts + and – denote the lower and upper limits of the smoothed transition and f_l is the liquid fraction. The effective heat capacity during phase change is given by:

$$c_{p,eff} = f_l c_{p,l} + (1 - f_l)c_{p,s} + L_m\frac{df_l}{dT} \tag{5}$$

where $c_{p,l}$ and $c_{p,s}$ are the liquid and solid specific heat capacities, respectively, and L_m is the latent heat of fusion. Analogously, effective thermophysical properties are computed as phase-weighted averages; for example, the effective thermal conductivity is defined as:

$$k_{eff} = f_l k_l + (1 - f_l)k_s \tag{6}$$

In summary, the inputs to the reference simulations are the fin geometry, boundary and initial conditions, thermophysical properties of the materials, mesh resolution, and the apparent heat capacity formulation. The outputs at each time step include the local temperature and liquid fraction fields in the PCM, as well as integrated quantities such as the overall liquid fraction, average temperature, and heat flux through the tube wall.

Due to the large number of finite elements required to resolve the detailed fin geometry, the governing equations must be solved locally at each element, resulting in significant computational cost. This makes the approach inefficient when only integrated quantities—such as total melting time or average heat flux—are required. A reduced or integrated modeling approach, capable of predicting these quantities without resolving the full spatial domain, would therefore substantially reduce computation time. The present reference simulations are therefore used as a benchmark for the development and validation of simplified, geometry-based performance models.

2.3. Effect of the fin material on phase change

If a given fin geometry (in this example Organic) is evaluated under the same boundary and initial conditions, the evolution of the phase change front strongly depends on the thermal properties of the fin material. Fig. 5 illustrates the temperature and liquid fraction fields for the quasi-isothermal material, aluminum, and stainless steel, using the thermophysical properties listed on Table 2.

In the quasi-isothermal case, heat diffusion within the fin is assumed to be instantaneous. The fin therefore is at a nearly uniform temperature equal to the boundary temperature, and no significant temperature gradient develops along its length. Under this condition, the phase change front grows at a constant normal distance from the fin surface. Consequently, the phase change front remains parallel to the fin contour, as schematically shown in Fig. 5b. The melting process is governed exclusively by the PCM thermal resistance.

For real materials, such as aluminum and stainless steel, a temperature gradient develops along the fin due to finite thermal diffusivity. The diffusivity ratio between the fin material and the PCM highlights this contrast: The ratio between the thermal diffusivity of aluminum and that of the eutectic mixture of KNO_3-$NaNO_3$ is near 490, whereas for stainless steel this ratio decreases to about 24. Although both materials are significantly more conductive than PCM, the internal fin resistance is no longer negligible. The temperature gradient within the fin is also time dependent, and modifies the shape of the phase change front.

In contrast to the quasi-isothermal case, where the phase change perimeter is maximal at the beginning of melting because the front develops simultaneously along the entire fin surface, real materials exhibit a delayed and spatially non-uniform melting behavior. Regions close to the tube heat up first, while distant fin sections contribute progressively as heat diffuses along the fin. Consequently, the perimeter does not peak at the initial stage but evolves dynamically as the internal fin temperature profile develops.

Within this scope, the problem involves two coupled transient mechanisms: transient phase change within the PCM; and transient heat

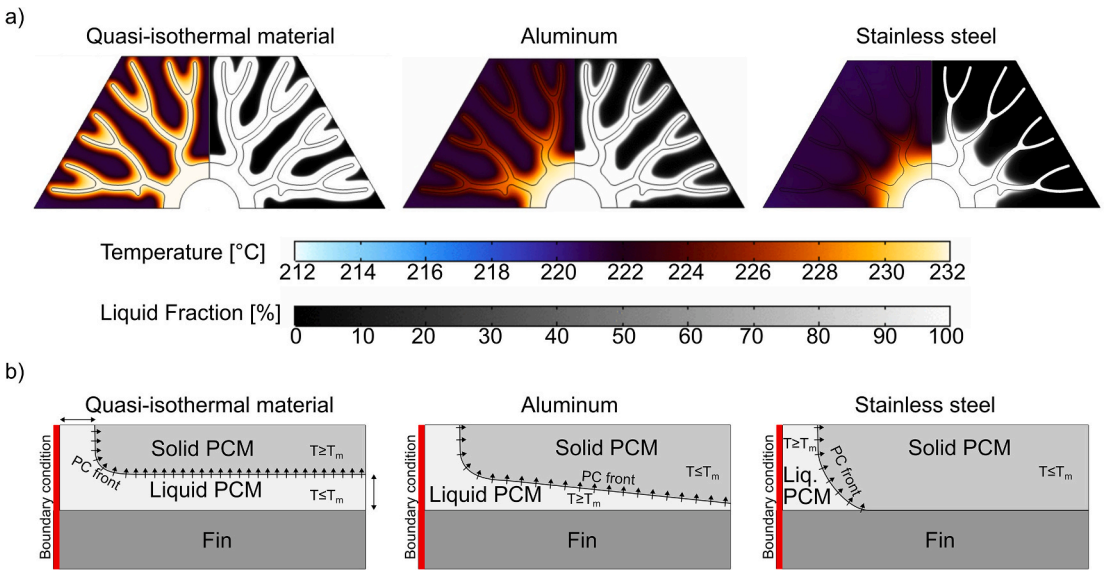

Fig. 5. Effect of the material of the fin. a) COMSOL simulation of the Organic profile using three different fin materials. Full melting time 950 [s] for the quasi-isothermal material, 1355 [s] for aluminum and 7720 [s] for stainless steel. b) Simplified scheme of the melting behavior.

diffusion within the fin. The interaction between these processes determines the heat transfer performance of the fin structure.

A classical way to quantify the impact of internal fin resistance is through the fin efficiency, defined as the ratio between the heat transferred by a real fin and the heat that would be transferred if the entire fin were at the base temperature. While this concept is well established for steady-state fins of simple geometry, analytical formulations for transient longitudinal fins remain limited. Existing studies typically address simplified configurations, and their extension to complex branched geometries is not straightforward [34].

For this reason, the quasi-isothermal case is introduced as a reference configuration in which fin resistance is negligible and the melting process can be expressed purely in terms of geometric distance distributions. This idealized reference serves as the absolute upper performance bound for fin geometry comparison. In the following sections, this formulation will be used to build the simplified model, demonstrating that this distance-based method provides a highly promising foundation for developing a fully non-isothermal derivation in future work.

2.4. Simplified model

2.4.1. Classical stefan formulation

To introduce the simplified model proposed in this study, it is useful to briefly recall the classical one-dimensional Stefan problem, schematically shown in Fig. 6 and thoroughly described by Alexiades and Solomon [11]. Consider the melting of a semi-infinite slab with constant thermophysical properties in each phase, initially fully solid at a uniform temperature below the melting point, $T < T_m$. When a constant temperature boundary condition $T_{boundary} > T_m$ is imposed at $x = 0$, the position of the phase change front will be given by:

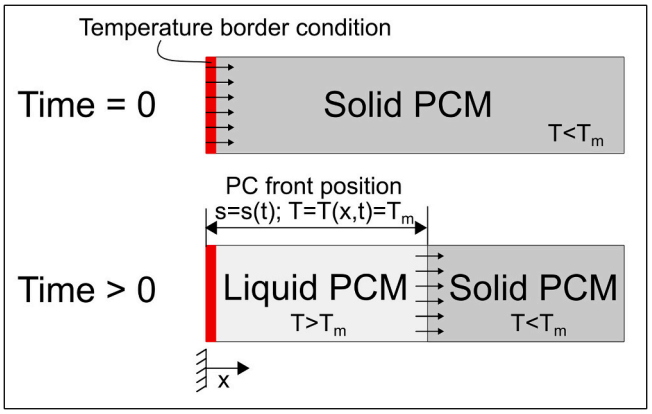

Fig. 6. Classic one-dimensional Stefan problem scheme.

$$s(t) = 2\lambda\sqrt{\alpha_l t} \tag{7}$$

where λ is the only positive root of the transcendental equation, α_l is the thermal diffusivity of the liquid phase, and t is time.

As established in Section 2.1, the operating conditions of the LHTES yield a small Stefan number ($Ste \approx 0.13$). Under the condition $Ste \ll 1$, the sensible heat required to raise the temperature of the liquid PCM is negligible compared to the dominant latent heat of fusion. This permits the use of the quasi-stationary approximation, which assumes a linear temperature profile across the newly formed liquid layer. Applying this approximation, the time (in seconds) at which the phase change front reaches a given position s will be:

$$t = \frac{s^2 \rho_{PCM} L_m}{2\, k_{PCM} \left| T_{boundary} - T_m \right|} \tag{8}$$

where ρ_{PCM} and k_{PCM} are the density and thermal conductivity of the PCM, respectively, and L_m is the latent heat of fusion. The corresponding heat flux $\dot{q}$ (in $\left[\frac{W}{m^2}\right]$) through the boundary "wall" becomes strictly dependent on the instantaneous conduction resistance of the melted layer:

$$\dot{q} = \frac{k_{PCM} \left| T_{boundary} - T_m \right|}{s} \tag{9}$$

These equations can be used to estimate the phase change times of simple, planar structures. However, a more complex mathematical description will be needed when fins are incorporated, since the transient heat transfer not only involves phase change, but also the transient heating through the fin.

2.4.2. Geometrical description of the fin profiles

In this study, two parameters will be defined to characterize the fin profiles. The first is the contact area between the fins and the PCM $A_{fin-PCM}$. In longitudinal fins, if its height is known as conceived on

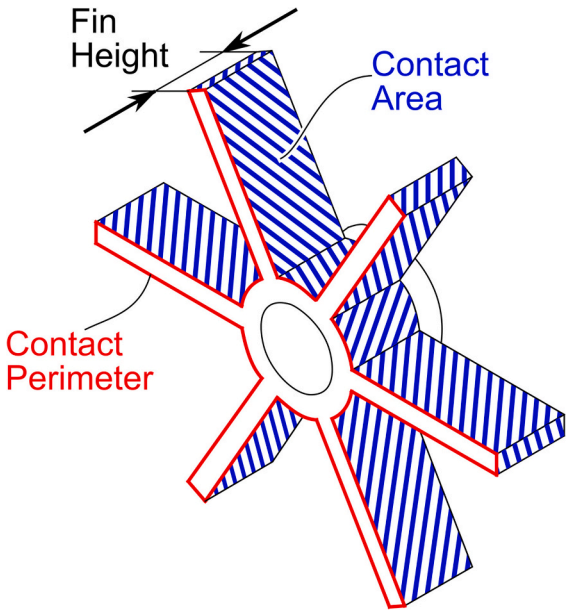

Fig. 7. Contact perimeter between PCM and fin.

Fig. 7, the contact perimeter P_{fin} can be calculated as:

$$P_{fin} = \frac{A_{fin-PCM}}{H_{fin}} \tag{10}$$

The second parameter is the heat transfer distance, defined as the shortest path through which heat is conducted from the tube boundary, through the fin material, and into the PCM. This concept is illustrated in Fig. 8, where the cross-section of the fin-PCM bundle for the "Snowflake" fin profile is discretized into elements of equal height and width.

The fin material distribution can be described through cumulative distributions of heat transfer distances. Two distance functions are defined: the distance between the tube boundary and fin elements $D_{fin-tube}$, and the distance between the PCM elements and the nearest fin element $D_{pcm-fin}$. In principle, the shorter the heat transfer paths, the faster the phase change.

The shortest distances are computed using Dijkstra's algorithm [35] applied to a connectivity graph representative of the discretized cross-section domain. This method ensures that the shortest conductive path is identified while accounting for the actual fin geometry. By mapping each PCM element exclusively to its nearest fin boundary, this geometric reduction inherently assumes that local melting is driven entirely by the closest heat source. The physical validity of assigning each PCM element exclusively to its nearest fin boundary relies on the low Stefan number ($Ste \approx 0.13$) characteristic of the case study of this paper. Because the sensible component is negligible compared to the latent one, heat diffusion predominantly follows the steepest temperature gradient, which aligns geometrically with the shortest distance to the fin. Consequently, the superposition of sensible heat fluxes from multiple surrounding fin branches is treated as a secondary effect and is neglected. The primary limitation of this assumption occurs within the narrow cavities of highly branched fins. In reality, melting in those regions would be slightly accelerated due to the superposition. By neglecting the superposition, the distance-based framework yields a mathematically conservative estimation of the melting speed. Ultimately, this assumption allows the original two-dimensional heat transfer problem to be transformed into a one-dimensional problem expressed in terms of cumulative distribution functions of the shortest heat transfer distances.

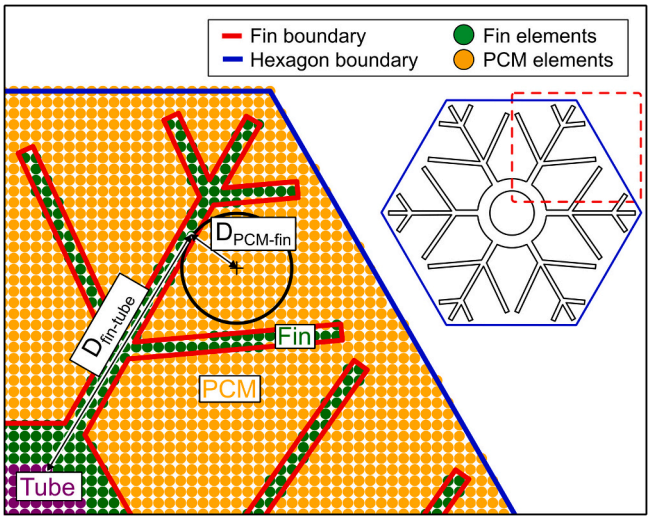

Fig. 8. Heat transfer distances concept using a coarse mesh.

After discretizing the cross-section into N elements (either PCM elements or fin elements, depending on the distance definition), and computing for each element i, a characteristic heat transfer distance D_i (either $D_{PCM-fin,i}$ or $D_{fin-tube,i}$), the cumulative distribution function (CDF) of the distances can be defined as:

$$CDF(d) = \frac{1}{N}\sum_{i=1}^{N} H(d - D_i) \tag{11}$$

where H is the Heaviside step function, d is a distance threshold within D_i, and $CDF(d) \in [0, 1]$. This definition represents the fraction of elements whose heat transfer distance is smaller or equal to a given threshold and can be represented as shown by Fig. 13.

As long as the thermal diffusivity of the fin is higher than that of the PCM, this paper states that the cumulative distribution function of distances between PCM and fin is proportional to the liquid fraction development over time:

$$CDF\left(D_{PCM-fin}\right) \propto f_l \tag{12}$$

2.4.3. Quasi-isothermal formulation

In the case of the quasi-isothermal fin material, no temperature gradient exists within the fin, and the melting front advances solely as a function of the local distance to the fin boundary. Under this assumption, all PCM elements with $D_{PCM-fin} \leq s(t)$ are molten at time t. Therefore, the liquid fraction can be expressed as:

$$f_l(t) = CDF(s(t)) \tag{13}$$

Consequently, the distance threshold corresponding to a given liquid fraction is:

$$s = CDF^{-1}(f_l) \tag{14}$$

Since the phase change front advances parallel to the fin surface under the quasi-isothermal assumption (as shown on Fig. 5), all PCM elements located within a distance s from the fin surface are considered molten. As the front advances from s to $s + \Delta s$, a thin layer of PCM melts. This layer consists of all PCM elements whose distance to the fin lies within the interval $[s, s + \Delta s]$. The increments on the melted areas can be defined as:

$$\Delta A_s(s) = A_{elements\ in\ [s,s+\Delta s]} \tag{15}$$

Because the front propagates parallel to the fin boundary, this increment can be approximated geometrically as:

$$\Delta A_s(s) \approx P_s(s)\Delta s \tag{16}$$

where $P_s(s)$ is the perimeter of the phase change front. Rearranging:

$$P_s(s) \approx \frac{\Delta A_s(s)}{\Delta s} \tag{17}$$

Taking the limit, the phase change front perimeter equals the rate of change of melted area with respect to the front distance:

$$P_s(s) = \frac{dA_s}{ds} \tag{18}$$

In the simplified discretized model, the increments are dependent on the element size. The perimeter is estimated by counting the number of elements whose distance lies within a small interval $[s, s + \Delta s]$ and multiplying that count by the element size:

$$P_s(s) \approx n(s)\Delta \mathrm{x} \tag{19}$$

where $n(s)$ is the number of elements within the considered distance bin and Δx is the grid spacing.

The total heat rate transferred across the phase change front is therefore proportional to the phase change perimeter. Expressed relative to the internal tube perimeter P_{tube}, the normalized heat flux through the internal tube boundary is:

$$\dot{q} = \frac{k_{PCM}\left|T_{boundary} - T_m\right|}{s}\ \frac{P_s(s)}{P_{tube}} \tag{20}$$

2.4.4. Definition of the time-ratio fin efficiency

In the literature, the fin efficiency η_{fin} is defined as the ratio between the actual heat transferred by the fin (in Watts) $\dot{Q}_{real}$, to the maximum possible heat that could be transferred if the entire fin were at the base temperature (isothermal case) $\dot{Q}_{iso}$ [36]. While this definition is standard for steady-state applications with constant convective boundary conditions, its direct application to transient LHTES systems presents significant physical and mathematical challenges.

First, due to the transient behavior comparing their instantaneous heat rates at the same chronological time t evaluates the system at fundamentally different melting states. To ensure a thermodynamically fair comparison, the performance must be evaluated at equivalent physical states, parameterized by the transient liquid fraction f_l.

Second, using an instantaneous fin efficiency ratio evaluated at a specific liquid fraction introduces extreme mathematical sensitivity. As the liquid fraction approaches 1, the thermal driving forces decrease, and the instantaneous heat transfer rates for both the real and quasi-isothermal cases approach zero. Dividing these vanishing quantities creates mathematical singularities and non-physical artifacts in the efficiency curves.

To resolve these limitations, a time-ratio fin efficiency η_{time} is proposed in this study. This metric evaluates the time-averaged heat transfer rate $\overline{\dot{Q}}$ required to reach a specific liquid fraction. It is defined as the total thermal energy $E(f_l)$ absorbed by the control volume divided by the elapsed melting time $t(f_l)$. Because the latent heat of the PCM overwhelmingly dominates the overall energy balance (characteristic of low Stefan number applications), the minor differences in sensible heat capacity between the different fin materials are thermodynamically negligible. Consequently, the total thermal energy required to reach a given liquid fraction can be treated as equivalent across all material cases. This allows the energy terms to cancel out, simplifying the equation entirely to the inverse ratio of their respective melting times:

$$\eta_{time}(f_l) = \frac{\overline{\dot{Q}}_{real}(f_l)}{\overline{\dot{Q}}_{iso}(f_l)} = \frac{\left(\frac{E}{t}\right)_{real}(f_l)}{\left(\frac{E}{t}\right)_{iso}(f_l)} = \frac{t_{iso}(f_l)}{t_{real}(f_l)} \tag{21}$$

where $t_{real}(f_l)$ and $t_{iso}(f_l)$ denote the respective times required for each configuration to reach the target liquid fraction f_l of 1. By evaluating the time-averaged performance rather than instantaneous thermal gradients, this approach effectively filters out the transient noise induced by local morphological changes of the melt front.

While total melting time remains the primary performance indicator for LHTES systems, quantifying the transient thermal penalty within the fin material provides a necessary additional dimension for geometric optimization. Therefore, the time-ratio efficiency η_{time} is introduced as an initial approach to capture the effect of internal conduction resistance through the fin. Ultimately, establishing a robust transient efficiency metric is intended to serve as a foundation for incorporating non-isothermal fin behavior into the simplified geometric model presented previously.

3. Results and discussion

The results of the simulations will be expressed using the liquid fraction and heat flux for each of the fin profiles, first for the reference case using aluminum fins, then the results of the quasi-isothermal material obtained by both the reference and the simplified model, and finally the fin efficiency indicator as an insight for future research.

3.1. Reference simulation and grid independence

Fig. 9 shows the PCM liquid fraction and heat flux through the interior of the tube for the four studied fin profiles. If the profiles are ordered from fastest to slowest phase change speed the result would be: 24-Branch-Star with 1130 s, Organic with 1355 s, Snowflake with 1885, and 6-Branch-Star with 5785 s.

Because of the assumptions used in this study, there should be no difference between melting and solidification heat flux and phase fraction results other than the obvious change of sign and the solidification case focusing on the solid fraction. These results will only focus on the melting case.

To demonstrate the independence of the numerical results from the mesh resolution, a grid independence study was performed using the Organic fin profile. Three simulations with an increasing number of elements during the melting process are compared in Table 3. For all remaining fin profiles, the same grid configuration as case #4 was adopted in the reference COMSOL simulations.

Fig. 10 presents the results obtained with the mesh configurations listed in Table 3. As expected, the computational time increases as the element size is reduced; however, the predicted liquid fraction and heat flux remain virtually unchanged. The differences between the curves are minimal and only become noticeable when a zoomed-in time interval is considered, confirming that the solution is mesh independent. All calculations were carried out on a Lenovo ThinkPad T14 Gen 4 laptop equipped with an Intel® Core™ i7-1355U processor and 16 GB of RAM.

In addition to grid independence, the temporal sensitivity of the model was managed using the COMSOL BDF (Backward Differentiation Formula) adaptive solver. To ensure high numerical precision, a strict relative tolerance of 10^{-5} was used. This parameter controls the local error estimation, forcing the solver to dynamically reduce the internal time steps whenever the physical gradients, such as the heat flux at the tube-fin interface, change rapidly. While results were exported at fixed intervals (e.g., 5 s) to manage data storage, the adaptive nature of the BDF solver ensures that the underlying transient physics are resolved with a much higher temporal resolution than the stored output suggests.

3.2. Geometric characterization of the fin profiles

Figure 11 shows the spatial distribution of the minimum distance between each PCM elements and its nearest fin boundary, $D_{PCM-fin}$. Fin profiles with a more homogeneous material distribution, such as Organic and 24-Branch-Star, show a relatively narrow distance spectrum, with maximum distances below 6 mm. In contrast, the 6-Branch-Star profile, that has a concentrated fin material distribution and large PCM regions between branches, presents significantly larger maximum distances, reaching approximately 18 mm. In all cases, the colormap

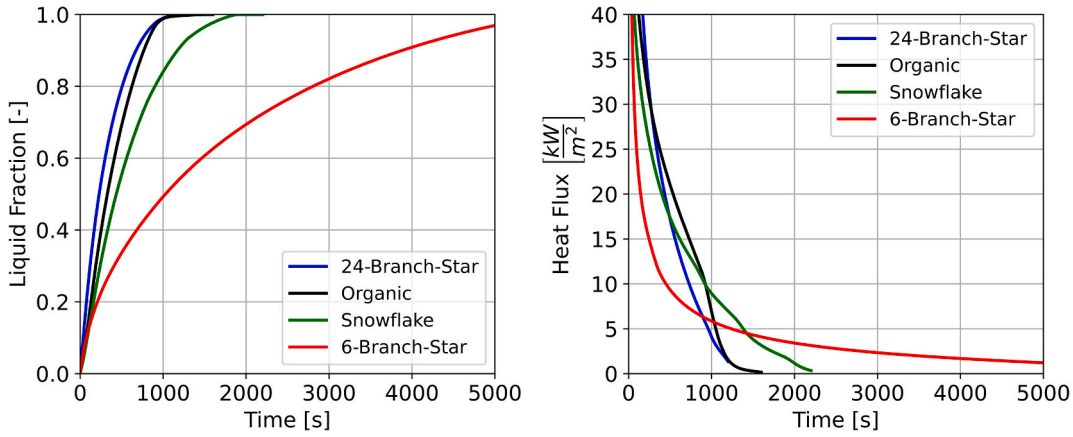

Fig. 9. Results of the reference melting COMSOL simulation using aluminum fins.

Table 3
Comparison of three COMSOL simulations of the melting using the Organic profile as benchmark and their effect on the computation time.

Control simulation	#1	#2	#3	#4
Maximum element size [mm]	4.00	0.45	0.18	0.09
Minimum element size [mm]	0.400	0.070	0.010	0.005
Number of elements	9052	12,910	47,620	284,966
Boundary elements	1371	1675	2928	5296
Computation time [s]	114	160	555	2141
Computation time [mm:ss]	01:54	02:40	09:11	35:41
$\frac{\textit{Simulated time}}{\textit{Computation time}}$	14.03	10	2.882	0.747

resembles the paths the phase change follows.

Figure 12 shows the minimum distance from each fin element to the nearest tube boundary, $D_{fin-tube}$. This distance characterizes the conductive path within the fin material and reflects how effectively heat can be transported from the tube to different regions of the fin structure.

Fig. 13 shows the cumulative distribution functions calculated through Eq. (11). The highly branched profiles (24-Branch-Star, Organic, and Snowflake) exhibit steep curves, indicating that the vast majority of the PCM mass is located within a distance shorter than 8 mm from the fin boundary. In contrast, the 6-Branch-Star profile exhibits a significantly broader distribution and large un-finned cavities. The distances throughout the fin to the tube have a remarkably similar distribution, with all profiles reaching their maximum conduction lengths near 40 mm. This contrast between the CDF's curves suggests that the spatial distribution of the fin within the PCM acts as the primary geometric differentiator governing the phase change dynamics. There is a clear resemblance between the liquid fraction shown in Fig. 9, and the cumulative distribution function plot for the distance between PCM-fin shown here.

Table 4 summarizes the geometric characterization of the evaluated fin profiles. As previously stated, all profiles share the same cross-sectional area (fin fraction), tube radius, and outer hexagonal boundary, differing exclusively in the spatial distribution of the aluminum. To quantify this distribution, the total contact perimeter P_{fin} and the average distance between PCM and fin $\overline{D}_{PCM-fin}$, and the average distance from the fin to the tube $\overline{D}_{fin-tube}$ were calculated and compared against the total melting times obtained from the COMSOL reference numerical model.

Fig. 14 shows the correlation of the proposed parameters and the total melting time for each fin. Regressions were applied to both datasets to evaluate their predictive reliability, quantified by the coefficient of

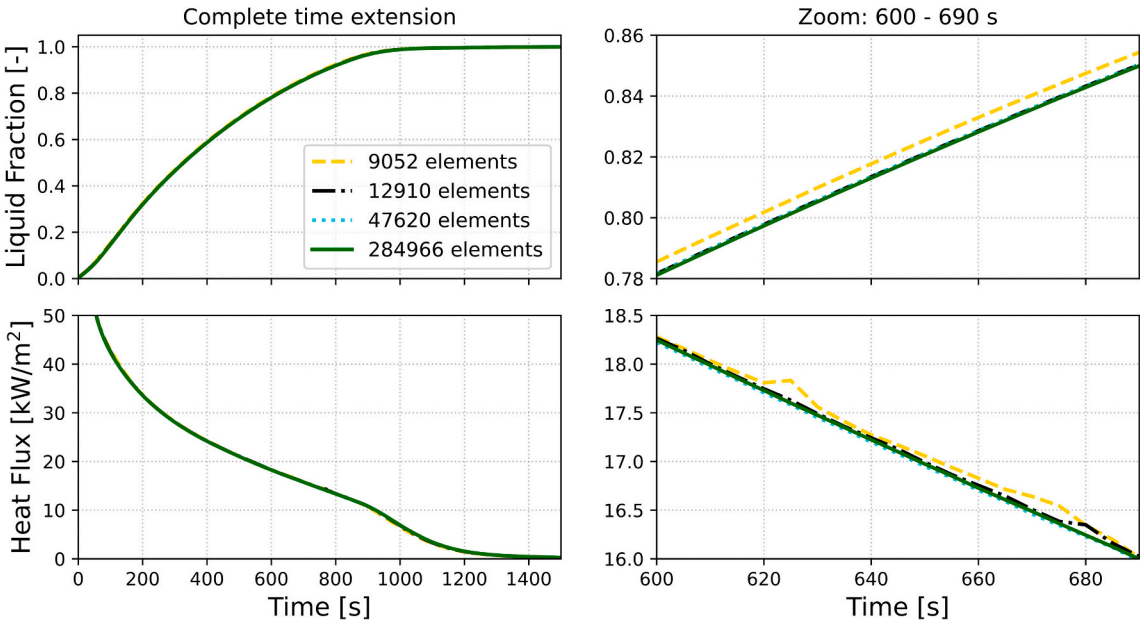

Fig. 10. Grid independence plot for the Organic profile using an increasing number of elements.

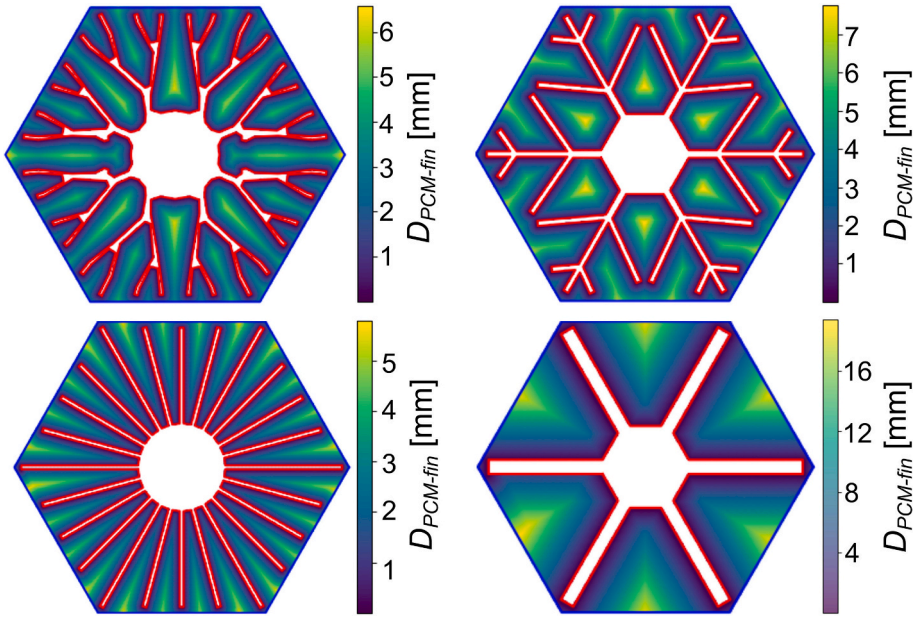

Fig. 11. Colormaps for the distance between the PCM elements and the nearest fin element $D_{PCM-fin}$.

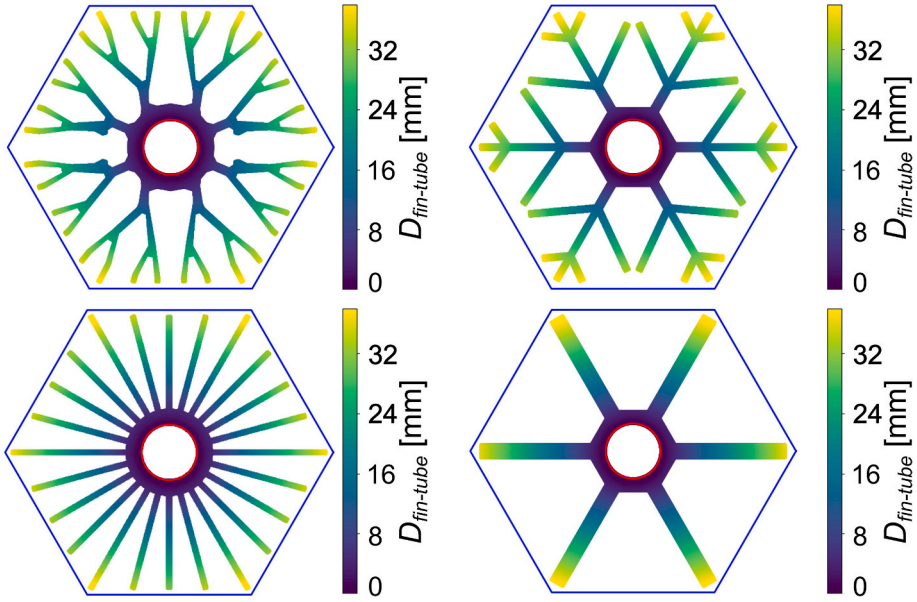

Fig. 12. Colormaps for the distance between the tube boundary and fin elements $D_{fin-tube}$.

determination (R^2), which represents the proportion of the variance in the melting time that is predictable from the respective geometric parameter.

The contact perimeter exhibits a strong non-linear inverse trend with melting time. As a general design guideline, for a given volume of fin material, the fin perimeter (or contact area between PCM-fin) should be maximized to reduce the melting time. The relation between the melting time and perimeter can be described with a power-law regression ($y = a{\cdot}x^b$), which was calculated using a logarithmic transformation. The resulting curve fits the data with high accuracy ($R^2 = 0.9960$).

In contrast, the average distance between the PCM and the fin $\overline{D}_{PCM-fin}$ demonstrates a directly proportional, perfectly linear correlation ($R^2 = 1.0000$). As a consequence, $\overline{D}_{PCM-fin}$ also serves as a robust geometric predictor for the melting behavior.

The third parameter, representing the average distance between the fin and the tube $\overline{D}_{fin-tube}$, shows no direct correlation with the melting time. This lack of correlation is physically consistent, the internal conduction path length does not govern the overall phase change speed, which is overwhelmingly dominated by the PCM thermal resistance. Finally, while the predictive capabilities $\overline{D}_{PCM-fin}$ are highly promising, evaluating a larger dataset of fin profiles will be necessary in future studies to determine if these tendencies are applicable across a broader geometric design space.

To further discuss the expected magnitude of convective effects and justify the conduction-driven assumption, the magnitude of natural convection can be estimated using the convective enhancement factor proposed by Vogel and Johnson. In confined vertical enclosures, the strength of the buoyancy-driven flow is governed by the Rayleigh number, $Ra = \frac{g\,\beta\,\Delta T\,W_c^3}{\nu\alpha}$, which scales with the cube of the characteristic cavity width (W_c). Approximating W_c as twice the average PCM-to-fin

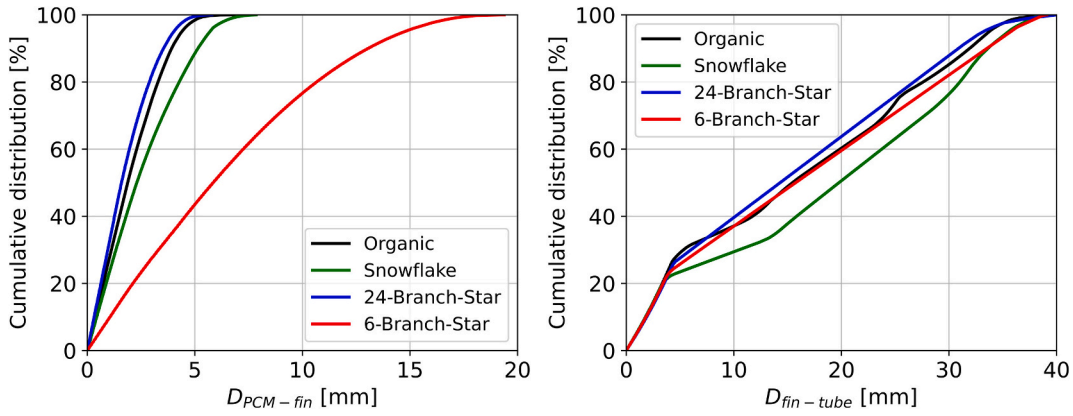

Fig. 13. Cumulative distribution function for the distances $D_{PCM-fin}$ (left) and $D_{fin-tube}$ (right).

Table 4
Results of the characterization of the fin profiles.

Fin Profile	24-Branch-Star	Organic	Snowflake	6-Branch-Star
A_{fin} $[mm^2]$	770			
f_{fin} [%]	13.2			
Tube internal radius [mm]	8			
Tube external radius [mm]	12.326			
Hexagon internal radius [mm]	41			
Hexagon external radius [mm]	47.34			
PCM and tube height [mm]	15			
P_{fin} [mm]	1480	1291	1078	463
$\overline{D}_{PCM-fin}$ [mm]	1.783	2.038	2.579	6.497
$\overline{D}_{fin-tube}$ [mm]	15.251	15.882	18.628	16.539
Melting time [s]	1130	1355	1885	5785

distance ($W_c = 2\,\overline{D}_{PCM-fin}$), the highly branched profiles (24-Branch-Star, Organic, and Snowflake) exhibit cavity widths below 5.2 mm, restricting their Rayleigh numbers strictly below 10^4. At this scale, viscous drag between opposing solid boundaries heavily suppresses convective currents. As demonstrated in the reference literature, the Organic profile yields an average convective enhancement factor near $\varepsilon = 1.05$, representing merely a 5% deviation from pure conduction. In contrast, the 6-Branch-Star yields an average cavity width of approximately 13 mm and $Ra \approx 1.55{\cdot}10^5$. While this concentrated geometry is more susceptible to natural convection, the literature establishes an upper enhancement limit of $\varepsilon < 2.0$ for similar scales. Furthermore, increasing vertical tube height actively decreases this convective enhancement. Therefore, in full-scale commercial storage units (e.g. 6 m height), the influence of natural convection is further suppressed by merged boundary layers, confirming the pure conduction model as a conservative baseline.

3.3. Comparison between reference and simplified simulation using isothermal fins

Fig. 15 shows the evolution of the PCM liquid fraction and the corresponding heat flux through the interior tube boundary for the four fin profiles on the quasi-isothermal case. As in this case, the resistance of the fin is neglected, the prediction of the simplified distance-based model demonstrates an excellent dynamic agreement with the reference COMSOL simulation through the bulk of the phase change process for all evaluated geometries.

To quantitatively evaluate the predictive capabilities of the simplified geometric model against the reference 2D COMSOL simulations, error metrics and computational times were extracted and are summarized in Table 5. Here, the melting time error Δt_m, maximum liquid fraction deviation $\Delta f_{l,max}$, mean absolute error for the liquid fraction $\overline{\Delta f_l}$, heat flux maximum deviations $\Delta \dot{q}_{max}$, mean absolute error for the heat flux $\overline{\Delta \dot{q}}$, computational time in COMSOL $t_{comp,COMSOL}$, computational time of the simplified model $t_{comp,simplified\ model}$, and the speedup ratio R_{speed} of the reference to the simplified approach are shown.

To isolate the dynamic agreement from the asymptotic behavior of phase change, Δt_m was evaluated at a 0.9 liquid fraction threshold. Under this criterion, the simplified model predicts the melting times within a 4.3% to 15.4% margin. The model demonstrates exceptional

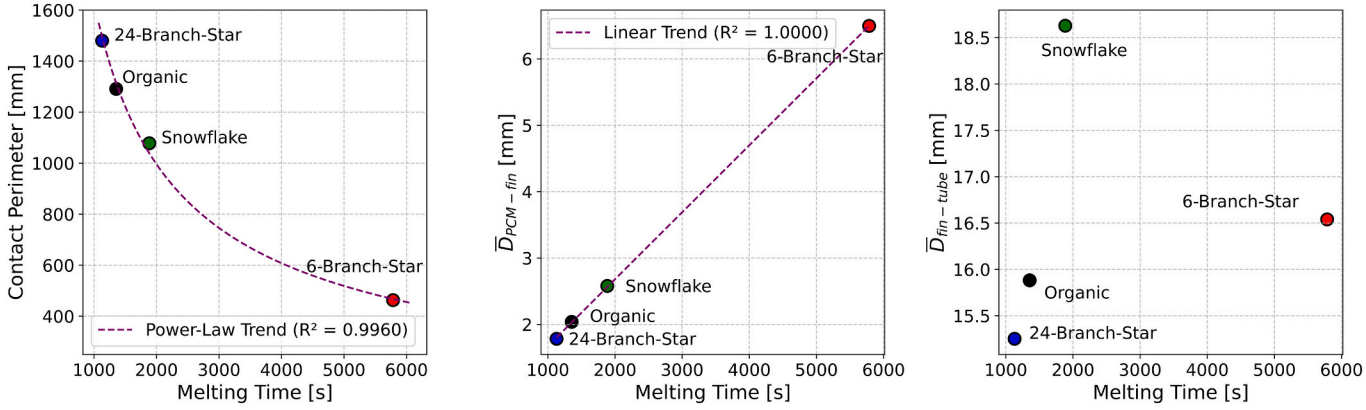

Fig. 14. Tendencies found for the proposed parameters with respect to the melting time.

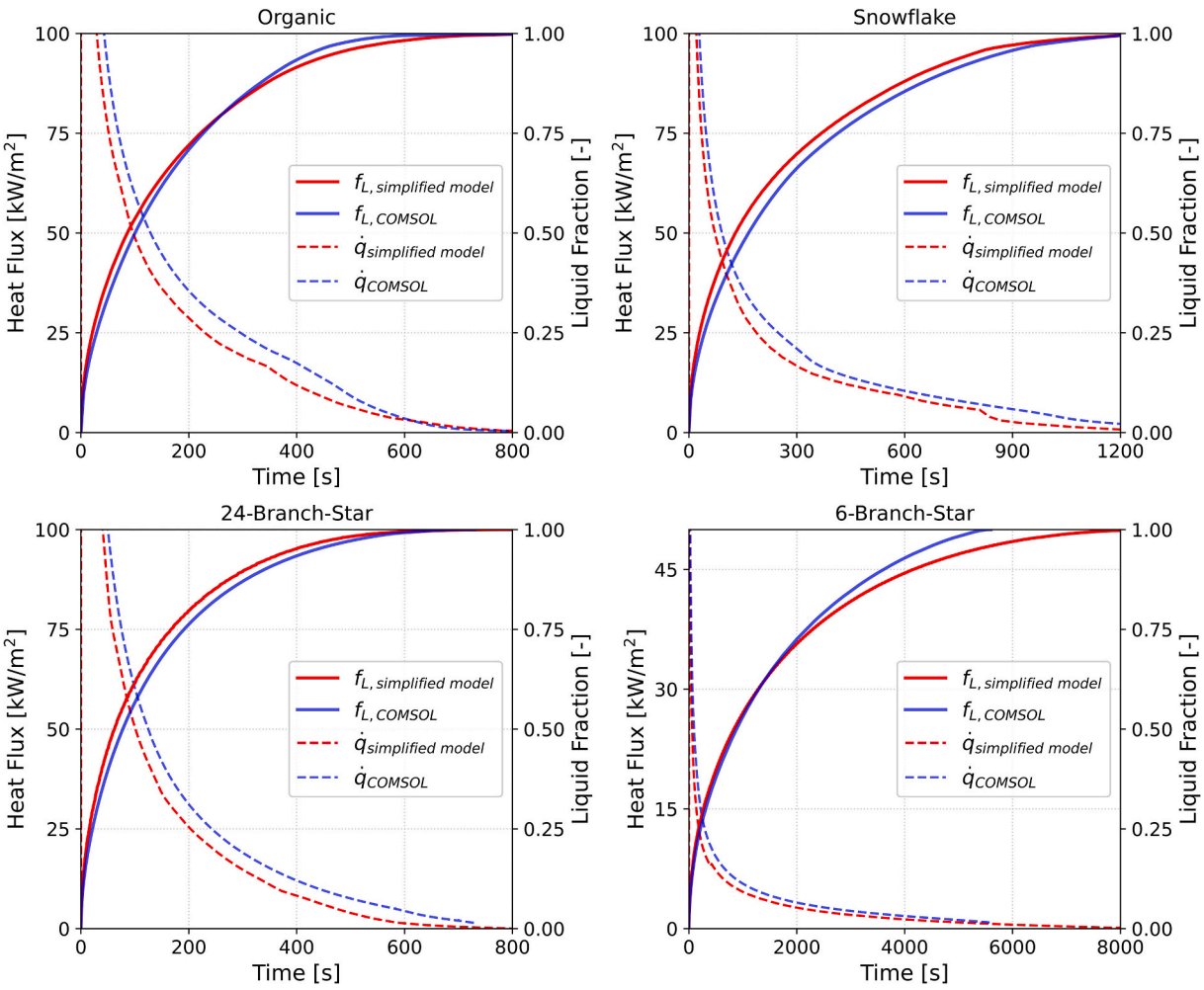

Fig. 15. Comparison between the results of liquid fraction and heat flux for each profile given by the simplified model and by COMSOL for the quasi-isothermal case.

Table 5
Global error metrics of the results obtained by the reference and simplified models.

Fin Profile	24-Branch-Star	Organic	Snowflake	6-Branch-Star
Δt_m [%]	9.98	4.30	8.97	15.36
$\Delta f_{l,max}$ [−]	0.0567	0.0451	0.0591	0.0454
$\overline{\Delta f_l}$ [−]	0.0222	0.0084	0.0211	0.0254
$\Delta \dot{q}_{max}$ [kW m^{-2}]	16.03	13.99	10.60	7.18
$\overline{\Delta \dot{q}}$ [kW m^{-2}]	4.73	2.22	2.51	0.83
$t_{comp,COMSOL}$ [hh:mm:ss]	00:23:25	01:17:18	00:31:39	01:05:08
$t_{comp,simplified\ model}$ [s]	7.7	34.9	24.6	29.6
R_{speed} [−]	183	133	77	132

transient agreement for the liquid fraction, yielding a mean absolute error of less than 0.026 across all profiles. This indicates that, on average, the instantaneous volume prediction deviates by less than 2.6% from the computationally intensive reference.

Similarly, a threshold of 50 s was applied for the heat flux comparison to avoid the initial peak when time is near 0. This exclusion bounds the error analysis to the physical propagation of the melting front. Here, $\overline{\Delta \dot{q}}$ remains strictly bounded between 0.83 and 4.73 [kW m^{-2}], while $\Delta \dot{q}_{max}$, which still corresponds to the initial times, lies between 7 and 16 [kW m^{-2}]. The low errors verify that the geometric CDF framework accurately captures the instantaneous rate of thermal diffusion across the evolving solid-liquid interface.

The most profound advantage of the proposed geometric approach lies in its computational efficiency. While the reference simulations required between 20 and 80 min, the simplified model was able to compare the geometries in less than 35 s. This yields a considerable speedup ratio R_{speed}, ranging between 77 and 183 times. Given this reduction in computational cost paired with acceptable average predictive errors, the proposed framework acts as a highly reliable tool for the design of finned tube profiles, enabling the rapid evaluation required for parameterized optimization algorithms.

A fundamental highlight of the methodology validated above is its geometric universality. Unlike existing quasi-analytical models that are restricted to specific, simple fin topologies, the present distance-based framework translates arbitrary 2D material distributions into 1D distance functions. This mathematical descriptor is universally applicable, remaining valid for profiles with significantly different fin fractions and larger outer diameters. However, its high predictive reliability without the need for empirical CFD recalibration relies strictly on operating within the conduction-driven regime. As established previously, combined convective effects become prominent when the average PCM-fin distance exceeds approximately 7.4 mm, as observed in the 230 mm diameter DSG profile [16]. At this scale, the convective enhancement factor approaches $\varepsilon = 2.0$, effectively reducing the phase change time by half. Therefore, the proposed framework is highly reliable precisely when the geometric distribution keeps these average distances low enough to suppress convection. Integrating macroscopic convective effects for sparse fin fractions, and utilizing this universal spatial descriptor to algorithmically optimize arbitrary fin geometries,

constitutes a compelling optimization problem for future research.

3.4. Extension to non-isothermal fins

The time-ratio fin efficiency η_{time} as a function of the liquid fraction f_l is presented in Fig. 16 for both aluminum (Alu) and stainless steel (SS) fins. To properly contextualize the efficiency curves, the absolute total melting times for each configuration are included directly within the figure legend. The results show a counterintuitive behavior: the geometries with the shortest absolute melting times exhibit the lowest fin efficiencies, and vice versa. For instance, the 6-Branch-Star using aluminum achieves an efficiency near 95% at the end of melting, yet it requires 5785 s to complete the phase change. This high efficiency indicates that the internal thermal resistance of its thick branches is negligible; its poor absolute performance is dictated entirely by its inefficient spatial distribution (large un-finned cavities). Conversely, the 24-Branch-Star achieves the fastest phase change (1130 s) but operates at merely 58% efficiency. Its spatial distribution provides a fast melting, but the needed slenderness of its branches creates a significant internal thermal bottleneck, and thus a lower fin efficiency.

By definition, the time-ratio efficiency remains strictly below unity throughout the entire melting process. Because a real fin with finite conductivity must overcome sensible heating and internal thermal resistance, its absolute melting time will always exceed that of the ideal, quasi-isothermal reference The impact of this internal bottleneck becomes severely pronounced when substituting aluminum with a lower-conductivity material. As shown by the dashed lines in Fig. 16, the efficiency of the highly branched profiles falls drastically when modeled with stainless steel. For the Organic and 24-Branch-Star profiles, the time-ratio efficiency drops below 10%, indicating that the heat flux fails to adequately reach the fin tips. Because the branches must be extremely thin to maintain the constant 13.2% fin fraction, the low thermal conductivity of stainless steel limits the heat's ability to reach deep into the geometry, heavily restricting the utilization of the optimized spatial distribution.

This severe internal conduction resistance observed in slender branches represents a techno-economical optimization problem for future investigations. For profiles like the Organic and 24-Branch-Star,

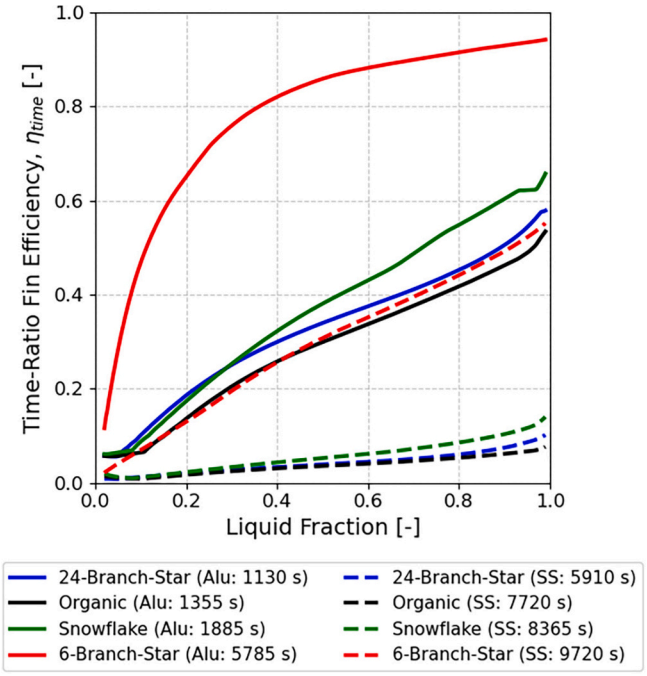

Fig. 16. Cumulative fin efficiency using the aluminum and quasi-isothermal material as expressed by Eq. (21).

the geometric potential is not fully realized. Substituting aluminum with a superior conductor, such as copper, would significantly reduce the thermal bottleneck and elevate their absolute performance toward their quasi-isothermal limits, but at a substantially higher material cost. Nevertheless, even without such upgrades, the superior geometric distribution of the highly branched profiles largely compensates for material downgrades. As demonstrated in Fig. 16, the 24-Branch-Star constructed from stainless steel completes the melting process in 5910 s, achieving a phase change time nearly equivalent to the 6-Branch-Star constructed from highly conductive aluminum (5785 s). This confirms that the spatial material distribution (the CDF) establishes the primary physical ceiling for heat transfer performance. If a low-conductivity material is required for system design, highly branched geometries remain imperative to achieve viable melting times, regardless of their low nominal efficiency.

Lastly, the time-ratio efficiency η_{time} quantifies the transient performance deviation between a real fin and the idealized quasi-isothermal assumption. For highly branched profiles, this deviation is substantial and demonstrates that the quasi-isothermal formulation alone is insufficient to predict their true behavior. To achieve a complete, geometry-based simplified model, these findings indicate that a transient correction factor, derived from metrics such as η_{time}, must be integrated to mathematically account for the internal thermal resistance of non-isothermal fins.

4. Conclusions

This study presented a novel, geometrically driven framework to characterize and evaluate longitudinally extruded finned tubes in Latent Heat Thermal Energy Storage (LHTES) units. Traditional design approaches often rely on the fin fraction, a metric that cannot independently describe the spatial distribution of the heat exchanger and typically requires additional parameters obtained through computationally intensive CFD simulations. To address this, four distinct fin profiles (24-Branch-Star, Organic, Snowflake, and 6-Branch-Star) with identical fin fractions were evaluated. By translating 2D fin cross-sections into 1D Cumulative Distribution Functions (CDFs) based on shortest heat transfer distances, a simplified transient model was developed and validated against reference numerical simulations.

The findings of this paper are summarized as follows:

- About the geometrically based parameters: Contact perimeter between PCM and fin P_{fin} presented a power-law correlation with the melting times, while the innovative average distance between PCM and fin $\overline{D}_{PCM-fin}$ presented a strictly proportional linear correlation. Both parameters are therefore proven to be suitable to build a robust, CFD-calibration-independent model. The analysis indicated that the average distance from the fin to the tube $\overline{D}_{fin-tube}$ has no correlation with the melting time, confirming that the phase change speed is strictly governed by the PCM thermal resistance.
- About the simplified approach: The proposed distance-based CDF approach successfully modeled the transient melting process of quasi-isothermal fins with high accuracy. The simplified model predicted the transient liquid fraction with a mean absolute error $\overline{\Delta f_l}$ of less than 0.026 across all profiles, while delivering a computational speedup ratio R_{speed} between 77 and 183 compared to the reference COMSOL simulations.
- About the extension to non-isothermal fins: The proposed time-ratio efficiency definition quantifies the performance gap between real fin materials and an idealized quasi-isothermal baseline. When a profile exhibits a high efficiency under this metric (e.g., the 6-Branch-Star), it indicates that the melting time is intrinsically bottlenecked by the fin geometry; even if a perfect thermal conductor were used, the phase change would not accelerate significantly. On the other hand, highly branched profiles are forced into slender geometries that

impose severe internal conduction penalties. While the current geometric CDF framework successfully models the quasi-isothermal baseline, formulating a purely geometric predictor to calculate this internal efficiency drop, without relying on reference numerical models, remains a crucial objective for future work.

- About topological independence: A significant implication of this methodology is that thermal performance is fundamentally governed by the distance distribution (CDF) rather than the specific topological classification (e.g., star, fractal, organic, etc.). Under conduction-dominated vertical configurations, distinct topologies sharing an identical CDF will exhibit identical melting dynamics. While existing literature frequently attributes thermal enhancements to specific topological designs, this framework demonstrates that topology is a secondary characteristic of the underlying fin material distribution. Consequently, the CDF serves as a comprehensive, topology-independent geometric descriptor, providing a highly reliable and fundamentally physical basis for the future optimization of fin profiles.

Ultimately, the resulting geometric parameters show high potential for their incorporation into simplified black-box models for LHTES units. By eliminating the reliance on reference numerical calibrations, this framework expands the computationally viable design space for storage-level assessments. Future work will focus on expanding the geometric dataset to fill the gaps between existing profiles. This parameterization will verify the universality of the observed correlations, paving the way for the rapid, algorithmic optimization of non-isothermal finned structures.

Declaration of AI-Assisted Technologies

During the preparation of this manuscript, Google Gemini was used to assist with Python code generation. All AI-assisted output was reviewed and edited and authors take full responsibility for the content of the publication. Besides, Grammarly was used to improve the readability, grammar and language of this article.

Declaration of competing interest

The authors declare that they have no known competing financial interests or personal relationships that could have appeared to influence the work reported in this paper.

Acknowledgements

Authors acknowledge the financial support given by the German Research Foundation (DFG) Priority Program: “Carnot Batteries: Inverse Design from Markets to Molecules” (SPP 2403), MultiPCM-Project Nr. 526035476. The first Author is grateful to colleagues of the Department of Thermal Processes Technologies (DLR-TT-TPT) for the inspiring discussions that lead to this work.

Data availability

The data that has been used is confidential.

References

[1] IEA, Batteries and Secure Energy Transitions, IEA, 2024, p. 67.
[2] A. Vandersickel, et al., IEA Task 36 Carnot Batteries Final Report, International Energy Agency, 2023.
[3] O. Dumont, et al., Carnot battery technology: a state-of-the-art review, J. Energy Storage 32 (2020).
[4] Z. Li, et al., Applications and technological challenges for heat recovery, storage and utilisation with latent thermal energy storage, Appl. Energy 283 (2021).
[5] W.-D. Steinmann, Thermal Energy Storage for Medium and High Temperatures, 2022.
[6] H. Mehling, L. Cabeza, Heat and cold storage with PCM, in: An up to Date Introduction into Basics and Applications, 2008.
[7] M. Zayed, et al., Recent progress in phase change materials storage containers: geometries, design considerations and heat transfer improvement methods, J. Energy Storage 30 (2020) 101341.
[8] S. Zhang, S. Mancin, L. Pu, A review and prospective of fin design to improve heat transfer performance of latent thermal energy storage, J. Energy Storage 62 (2023).
[9] T. Zhu, et al., A review on heat transfer enhancement of phase change materials using fin tubes, Energies 16 (2023).
[10] DLR, Entwicklung und Integration Thermischer Energiespeicher in Rinnenkraftwerken mit Solarer Direktverdampfung: Verbundvorhaben ITES-Schlussbericht, Deutsches Zentrum für Luft- und Raumfahrt, 2012.
[11] V. Alexiades, A.D. Solomon, Mathematical Modeling of Melting and Freezing Processes, Taylor & Francis, 1993.
[12] H.S. Carslaw, J.C. Jaeger, Conduction of Heat in Solids, 2nd ed, Oxford and the Clarendon Press, 1959.
[13] W. Beyne, et al., A predictive method for pipe in pipe, cylindrical modules and spherical packed bed latent thermal energy storage systems, J. Energy Storage 68 (2023).
[14] T. Bauer, Approximate analytical solutions for the solidification of PCMs in fin geometries using effective thermophysical properties, Int. J. Heat Mass Transf. 54 (23–24) (2011) 4923–4930.
[15] V.R. Voller, M. Cross, N.C. Markatos, An enthalpy method for convection/diffusion phase change, Int. J. Numer. Methods Eng. 24 (1) (1987) 271–284.
[16] J. Vogel, M. Johnson, Natural convection during melting in vertical finned tube latent thermal energy storage systems, Appl. Energy 246 (2019) 38–52.
[17] J. Vogel, M. Keller, M. Johnson, Numerical modeling of large-scale finned tube latent thermal energy storage systems, J. Energy Storage 29 (2020).
[18] N.H.S. Tay, M. Belusko, F. Bruno, An effectiveness-NTU technique for characterising tube-in-tank phase change thermal energy storage systems, Appl. Energy 91 (1) (2012) 309–319.
[19] A. Sciacovelli, F. Gagliardi, V. Verda, Maximization of performance of a PCM latent heat storage system with innovative fins, Appl. Energy 137 (2015) 707–715.
[20] A. Pizzolato, et al., Design of effective fins for fast PCM melting and solidification in shell-and-tube latent heat thermal energy storage through topology optimization, Appl. Energy 208 (2017) 210–227.
[21] A. Pizzolato, et al., Topology optimization for heat transfer enhancement in latent heat thermal energy storage, Int. J. Heat Mass Transf. 113 (2017) 875–888.
[22] R. Ge, et al., Additive manufacturing of a topology-optimised multi-tube energy storage device: experimental tests and numerical analysis, Appl. Therm. Eng. 180 (2020).
[23] Y. Wang, et al., Optimizing fin design for enhanced melting performance in latent heat thermal energy storage systems, J. Energy Storage 73 (2023).
[24] L. Dietz, I. Bürger, A. Gutierrez, Effect of steam flow parameters on the partial load behaviour of a PCM storage, J. Energy Storage 89 (2024).
[25] M. Johnson, , et al.TESIN Project Final Report, DLR Institute of engineering thermodynamics, Thermal Process Technology, 2022, pp. 70–75.
[26] J. Vogel, J. Felbinger, M. Johnson, Natural convection in high temperature flat plate latent heat thermal energy storage systems, Appl. Energy 184 (2016) 184–196.
[27] H. Pointner, W.-D. Steinmann, Experimental demonstration of an active latent heat storage concept, Appl. Energy 168 (2016) 661–671.
[28] J. Tombrink, D. Bauer, Demand-based process steam from renewable energy: implementation and sizing of a latent heat thermal energy storage system based on the rotating drum heat exchanger, Appl. Energy 321 (2022).
[29] D.J. Rogers, G.J. Janz, Melting-crystallization and premelting properties of sodium nitrate-potassium nitrate. Enthalpies and heat capacities, J. Chem. Eng. Data 27 (4) (2002) 424–428.
[30] R.M. DiGuilio, A.S. Teja, The thermal conductivity of the molten NaNO3-KNO3 eutectic between 525 and 590 K, Int. J. Thermophys. 13 (4) (1992) 575–592.
[31] J. Vogel, Influence of Natural Convection on Melting of Phase Change Materials, University of Stuttgart, 2019.
[32] K.M. Germany, Chemical Composition, Physical and Mechanical Properties of 1.4301 (X5CrNi18–10), 06.11.2025; Available from: https://facts.kloeckner.de/werkstoffe/edelstahl-werkstoffe/1-4301/, 2025.
[33] COMSOL-Multiphysics®. 2025, COMSOL AB: Stockholm, Sweden.
[34] A. Mostafavi, A. Jain, Thermal management effectiveness and efficiency of a fin surrounded by a phase change material (PCM), Int. J. Heat Mass Transf. 191 (2022).
[35] E.W. Dijkstra, A note on two problems in connexion with graphs, Numer. Math. 1 (1) (1959) 269–271.
[36] T.L.a.L. Bergman, S. Adrienne, Frank P. Incropera, David P. DeWitt, Fundamentals of Heat and Mass Transfer, 7th ed, John Wiley & Sons, 2011.